The Astrophysical Journal, 614:547–557, 2004 October 20

NEAR-INFRARED SPECTROSCOPY OF HIGH-REDSHIFT ACTIVE GALACTIC NUCLEI. I. A METALLICITY–ACCRETION RATE RELATIONSHIP

O. Shemmer,[1] H. Netzer,[1] R. Maiolino,[2] E. Oliva,[3] S. Croom,[4] E. Corbett,[4] and L. di Fabrizio[3]

Received 2004 March 28; accepted 2004 June 22

ABSTRACT

We present new near-infrared spectroscopic measurements of the Hβ region for a sample of 29 luminous high-redshift quasars. We have measured the width of Hβ in those sources and added archival Hβ width measurements to create a sample of 92 active galactic nuclei (AGNs) for which Hβ width and rest-frame UV measurements of N v λ1240 and C iv λ1549 emission lines are available. Our sample spans 6 orders of magnitude in luminosity and includes 31 radio-loud AGNs. It also includes 10 narrow-line Seyfert 1 galaxies and one broad absorption line quasar. We find that metallicity, indicated by the N v/C iv line ratio, is primarily correlated with accretion rate, which is a function of luminosity and Hβ line width. This may imply an intimate relation between starbursts, responsible for the metal enrichment of the nuclear gas, and AGN fueling, represented by the accretion rate. The correlation of metallicity with luminosity, or black hole (BH) mass, is weaker in contrast to recent results that were based on measurements of the width of C iv. We argue that using C iv as a proxy to Hβ in estimating $M_{\rm BH}$ might be problematic and lead to spurious BH mass and accretion rate estimates in individual sources. We discuss the potential implications of our new result in the framework of the starburst-AGN connection and theories of BH growth.

Subject headings: galaxies: abundances — galaxies: active — galaxies: nuclei — galaxies: Seyfert — galaxies: starburst — quasars: emission lines

1. INTRODUCTION

The determination of chemical abundances in active galactic nuclei (AGNs) provides a powerful tool to probe star-forming activity in galactic nuclei at present and in the early universe. Early metal abundance studies in AGNs utilized weak and broad intercombination lines, such as N iii] λ1750, N iv] λ1486, and O iii] λ1663, to determine metal abundances in the broad-line region (BLR) gas (Shields 1976). These early studies have found that BLR metallicity is about solar, with some luminous quasars reaching supersolar values. Hamann & Ferland (1993, hereafter HF93) found that emission-line ratios such as N v λ1240/C iv λ1549 (hereafter N v/C iv) can trace the BLR metallicity across a wide range of luminosity and BLR density (see also Hamann et al. 2002 for a more detailed model). HF93 also found that BLR metallicity determined in this way correlates with luminosity, in what they proposed as the metallicity-luminosity (*Z*-*L*) relationship in AGNs. Given the well-known relationship between AGN luminosity and black hole (BH) mass ($M_{\rm BH}$), HF93 suggested that the *Z*-*L* relationship can naturally lead to a *Z*-$M_{\rm BH}$ dependence, in analogy with the mass-metallicity relation observed in some elliptical galaxies (e.g., Trager et al. 2000).

Shemmer & Netzer (2002, hereafter SN02) have shown that once narrow-line Seyfert 1 galaxies (NLS1s) are introduced into the *Z*-*L* diagram, they deviate significantly from the *Z*-*L* relation by exhibiting high N v/C iv at low luminosity. A possible explanation is that N v/C iv is not an adequate metallicity indicator for NLS1s (and perhaps other AGNs). Otherwise, this implies that at least at low luminosity, the *Z*-*L* relation is more complex and cannot be a simple two-parameter dependence. According to SN02, BLR metallicity also depends on the width of Hβ, which is perhaps the best accretion rate (in terms of the Eddington ratio: $L_{\rm Bol}/L_{\rm Edd}$) indicator, and that this dependence may prevail also at the high-luminosity end. To test this hypothesis, we observed the near-infrared spectrum of a sample of 29 luminous $2 < z < 3.5$ quasars, with available N v/C iv data, in order to measure the width of their Hβ lines and thus deduce the accretion rate in these sources.

This paper is part of a two paper project describing near-IR spectroscopic measurements of luminous high-redshift quasars aimed at estimating $L_{\rm Bol}/L_{\rm Edd}$ and measuring the emission-line properties in such objects. In this (first) paper we describe the quasars' selection, their observations, and data reduction (§ 2). A description of the data analysis is given in § 3. In § 4 we summarize our main results concerning the broad emission lines, and in § 5 we discuss their potential implications. A summary of our main conclusions is given in § 6. A companion paper (Netzer et al. 2004, hereafter Paper II) addresses the complementary issue of the [O iii] and Fe ii lines in those sources.

2. SAMPLE SELECTION, OBSERVATIONS, AND DATA REDUCTION

We have selected a sample of 29 luminous quasars for our study on the basis of the following criteria:

1. Luminous ($L \gtrsim 10^{46}$ ergs s^{-1}) sources with expected *H* magnitudes $\lesssim$17 to allow high-S/N spectra on medium size telescopes.
2. Each source has an archived or published rest-frame UV spectrum that includes the N v and C iv emission lines, which are not subject to severe absorption.
3. Hβ is located in the observable IR bands, where it is least affected by atmospheric absorption.

[1] School of Physics and Astronomy and the Wise Observatory, Raymond and Beverly Sackler Faculty of Exact Sciences, Tel Aviv University, Tel Aviv 69978, Israel; ohad@wise.tau.ac.il, netzer@wise.tau.ac.il.
[2] INAF–Osservatorio Astrofisico di Arcetri, Largo Enrico Fermi 5, I-50125 Florence, Italy; maiolino@arcetri.astro.it.
[3] Istituto Nazionale di Astrofisica, Centro Galileo Galilei, and Telescopio Nazionale Galileo, P.O. Box 565, E-38700 Santa Cruz de la Palma, Spain; oliva@tng.iac.es.
[4] Anglo-Australian Observatory, P.O. Box 296, Epping, NSW 1710, Australia; scroom@aaoepp.aao.gov.au.

TABLE 1
Observation Log

Quasar Name	R.A. (J2000.0)	Decl. (J2000.0)	z[a]	z_{sys}[b]	H[c]	Observatory	Date
2QZ J001221.1−283630	00 12 21.1	−28 36 30	2.327	2.339*	16.6*	AAT	2003 Jul 17
2QZ J002830.4−281706	00 28 30.4	−28 17 06	2.406*	2.401	15.9*	AAT	2003 Jul 16
UM 667	00 47 50.1	−03 25 31	3.122	3.132	...	TNG	2003 Aug 18
LBQS 0109+0213	01 12 16.9	+02 29 48	2.343	2.349	15.3*	TNG	2002 Nov 8
[HB89] 0123+257[d]	01 26 42.8	+25 59 01	2.358	2.369	15.9*	TNG	2002 Aug 27
2QZ J023805.8−274337	02 38 05.8	−27 43 37	2.452*	2.471*	16.0*	AAT	2003 Jul 15
SDSS J024933.42−083454.4	02 49 33.4	−08 34 54	2.491	2.491	16.5	AAT	2003 Jul 16
[HB89] 0329−385[d]	03 31 06.3	−38 24 05	2.423	2.435	15.6*	AAT	2003 Jul 14
[HB89] 0504+030[d]	05 07 36.4	+03 07 52	2.463	2.473	...	TNG	2002 Nov 10
SDSS J100428.43+001825.6	10 04 28.4	+00 18 26	3.046	3.046	...	TNG	2003 Nov 13
TON 618[d]	12 28 24.9	+31 28 38	2.219	2.226*	13.9*	TNG	2003 Jun 4
[HB89] 1246−057	12 49 13.9	−05 59 19	2.236	2.240*	14.3*	TNG	2003 Jun 6
[HB89] 1318−113	13 21 09.4	−11 39 32	2.308	2.306	15.1*	TNG	2003 Jun 5
[HB89] 1346−036	13 48 44.1	−03 53 25	2.344	2.370*	15.1*	TNG	2002 Apr 5
SDSS J135445.66+002050.2	13 54 45.7	+00 20 50	2.511	2.531*	...	TNG	2004 Apr 1
UM 629	14 03 23.4	−00 06 07	2.462	2.460	16.0*	AAT	2003 Jul 16
UM 632[d]	14 04 45.9	−01 30 22	2.518	2.517	16.1*	TNG	2003 Jun 5
UM 642	14 10 26.4	−00 50 09	2.372	2.361	16.6*	TNG	2003 Jun 4
UM 645[d]	14 11 23.5	+00 42 53	2.269	2.257	...	TNG	2003 Jun 7
SBS 1425+606	14 26 56.1	+60 25 50	3.160	3.202	14.5*	TNG	2003 Aug 30
SDSS J170102.18+612301.0	17 01 02.2	+61 23 01	2.293	2.301*	16.4*	TNG	2003 Jun 4
SDSS J173352.22+540030.5	17 33 52.2	+54 00 30	3.425	3.428	15.7*	TNG	2003 Aug 30
[HB89] 2126−158	21 29 12.2	−15 38 41	3.268	3.282	14.9*	TNG	2003 Oct 15
[HB89] 2132+014[d]	21 35 10.6	+01 39 31	3.194	3.199	...	TNG	2003 Sep 5
2QZ J221814.4−300306	22 18 14.4	−30 03 06	2.384*	2.389	16.0*	AAT	2003 Jul 16
2QZ J222006.7−280324	22 20 06.7	−28 03 24	2.406	2.414	14.3*	AAT	2003 Jul 15
[HB89] 2254+024[d]	22 57 17.5	+02 43 18	2.081	2.083	15.9*	TNG	2003 Jun 16
2QZ J231456.8−280102	23 14 56.8	−28 01 02	2.392*	2.400	16.6	AAT	2003 Jul 17
2QZ J234510.3−293155	23 45 10.3	−29 31 55	2.360	2.382	16.5	AAT	2003 Jul 17

[a] Redshift taken from the NASA/IPAC Extragalactic Database (NED; http://nedwww.ipac.caltech.edu), except for values with asterisks, which were taken from the 2QZ archive.
[b] Systemic redshift determined from the peak of the [O III] λ5007 emission line. In cases where no [O III] emission was detected, Hβ was used instead (asterisks).
[c] Magnitudes with asterisks are 2MASS measurements, while others were obtained by photometric measurements using field comparison stars, whose magnitudes were taken from the 2MASS archive. Six sources do not have 2MASS magnitudes (or H images with comparison stars having 2MASS magnitudes), and their rest-frame optical fluxes were obtained from extrapolation of the rest-frame λ1450 flux.
[d] Radio-loud quasar.

According to these criteria, all of our quasars lie in a $2 < z < 3.5$ redshift range, with Hβ located in either the H or K band. Observations were done at the Anglo-Australian Telescope (AAT) in Australia and at the Telescopio Nazionale Galileo (TNG) in Spain. An observation log and quasar details appear in Table 1.

The observations at TNG were done with the Near Infrared Camera Spectrometer (NICS). Eight quasars were observed with a 1″ wide slit, and eleven were observed with a 0.″5 wide slit. During the observations the telescope was nodded along the slit and each spectrum was taken at 2–6 different positions along the spatial axis in order to perform the primary background subtraction. We used the HK grism to obtain the 1.4–2.5 μm wavelength range, which provides an almost uniform dispersion of 11.2 Å pixel^{-1} throughout this range. This results in a resolving power of $R \sim 500$ (1″ slit) or $R \sim 1000$ (0.″5 slit), slightly increasing toward the red. Each night, spectra of one or two standard O stars were taken as close as possible in time and in air mass to the quasars to allow the removal of telluric absorption features from the quasars' spectra.

The spectroscopic observations at AAT were done with the second-generation Infrared Imager and Spectrograph (IRIS2) and a 1″ wide slit. During the observations the telescope was nodded along the slit in an ABBA sequence; thus, each spectrum was broken into a set of four frames to allow primary background subtraction. We used the Sapphire-H grism together with an H filter to obtain the 1.54–1.90 μm wavelength range,[5] with a dispersion of 3.4 Å pixel^{-1} and a resolution of $R \sim 2500$. Standard stars of spectral types O, B, and G were observed each night to remove telluric features from the quasars' spectra. We also used the imaging mode of IRIS2 to take H-band images of our quasars. H magnitudes for the quasars were obtained by relative photometry and comparison with H magnitudes of nearby stars taken from the Two Micron All Sky Survey (2MASS) archive.[6] Seven of the quasars also had H magnitudes in the 2MASS archive. Nonsystematic differences of up to ~0.5 mag were found between these magnitudes and the magnitudes obtained by the relative photometry. This may be mainly due to increased photometric errors near the edge of the 2MASS detection limit.

[5] Normally, this setup allows a coverage of the 1.485–1.781 μm range, i.e., the entire H band; however, a misplacement of the grism in the filter wheel during our run resulted in a short-wavelength cutoff.
[6] See http://www.ipac.caltech.edu/2mass.

The two-dimensional spectra (quasars and standard stars) from both observatories were reduced using standard IRAF[7] routines. All spectra were pair-subtracted to remove most of the background, which is swamped by strong telluric features, such as OH emission, leaving some residuals perpendicular to the spatial axis. For each observatory we used a lamp spectrum as a flat-field image to correct each spectrum for pixel-to-pixel variations. Each spectrum was fitted by a low-order polynomial, and a secondary background subtraction, along the dispersion, was carried out. An extraction window of $1''$ ($0''.5$) was used to extract each of the AAT (TNG) spectra, respectively. Wavelength calibration was achieved using Xe and Ar arc lamps. Finally, all spectra were rebinned to a common resolution of $\sim$600 km s^{-1}, matching the resolution of the TNG spectra taken with the $1''$ slit.

The spectral shape of the quasars was recovered by dividing each spectrum by a spectrum of a standard star, after the stellar absorption features were carefully removed. The quasar/star ratio was then multiplied by a stellar model in the form of a blackbody curve, with a temperature corresponding to the star's tabulated spectral type. Some of our standard stars have spectra that appear in the library of near-IR stellar spectra of Lançon & Rocca-Volmerange (1992). This enabled the removal of major intrinsic absorption features in our standard stars and also allowed us to compare our stellar model to the archived data. Flux calibration of the quasars was obtained by comparing synthetic H and K magnitudes of the quasars (by integrating counts across the dispersion) to the observed H magnitudes (see Table 1) and using the flux density of Vega as the zero-point flux.

Our flux calibration may be subject to relatively large uncertainties emerging from different atmospheric absorption between a quasar and its corresponding standard star. This uncertainty increases for the AAT spectra, as those are cut off short of the H-band blue end. For those spectra we integrated the predicted counts after extrapolating the continuum (fitted by a linear function) beyond $\sim$1.55 μm. We also used the b_J magnitudes of the 2QZ quasars to check for consistency with our derived rest-frame optical fluxes, by converting those magnitudes to observed 4400 Å fluxes and extrapolating them to 5100 Å assuming a fiducial quasar continuum function of the form $f_\nu \propto \nu^{-0.5}$. We found that our H and b_J magnitudes (reflected to the observed H band) were consistent to within $\pm$0.25 mag. We note that those two magnitudes were measured at different epochs, separated by $\sim$20 yr in time, thus constraining the variability amplitude of each quasar to $\sim$25% over a timescale of $\sim$6 yr in the rest frame (although there is a scope for variability within this long period of time). Luminosities were obtained by using the following cosmological parameters: $\Omega_\Lambda = 0.7$, $\Omega_m = 0.3$, and $H_0 = 70$ km s^{-1} Mpc^{-1}.

In addition to our 29 sources, we added to our sample two quasars, LBQS 0256−0019 and LBQS 0302−0000, for which rest-frame UV spectra were available from the Sloan Digital Sky Survey (SDSS; Stoughton et al. 2002) archive, and a high-quality rest-frame optical spectrum including Hβ was kindly provided by M. Dietrich (2003, private communication; see Dietrich et al. 2002). As a result, our high-redshift sample consists of 31 luminous quasars.

Our new sample was complemented by 61 $z < 2$ AGNs, from the original SN02 sample, all with published Hβ data. Altogether this sample comprises 92 sources, including 10 NLS1s, with N v, C iv, and Hβ information. One of our sources is a broad absorption line quasar ([HB89] 1246−057), based on its UV spectrum, and 31 of our sources (eight at $2 < z < 3.5$, and the rest at low z including one NLS1) were identified as being radio-loud quasars (RLQ), following the discrimination between RLQ and radio-quiet quasars (Kellerman et al. 1989) and using optical and radio fluxes from Veron-Cetty & Veron (2003).

[7] IRAF (Image Reduction and Analysis Facility) is distributed by the National Optical Astronomy Observatory, which is operated by AURA, Inc., under cooperative agreement with the National Science Foundation.

3. MEASUREMENTS AND DATA ANALYSIS

3.1. Hβ *Width*

The Hβ region in the final spectra was fitted with a model consisting of a linear continuum, the Boroson & Green (1992) Fe ii emission template, and a multi-Gaussian fit to the emission lines. We also fitted the Hα region in the TNG spectra (where present) in the same way, but these data are left out of the current analysis. In the first step we fitted a linear continuum and one Gaussian to Hβ to get a rough estimate of its FWHM. The next step was to broaden the Fe ii emission template by convolving it with a Gaussian whose width was identical to FWHM (Hβ). We then fitted the spectrum with a linear continuum, the broadened Fe ii template, shifted in flux by a scaling factor, and multi-Gaussian components for the emission lines. Two Gaussians with differing widths were assigned to Hβ, and two Gaussians with identical widths were assigned to the two [O iii] $\lambda\lambda$4959, 5007 lines. The fluxes of the [O iii] lines were constrained to the theoretical ratio I([O iii] λ5007)/I([O iii] λ4959) = 2.95, and the widths of the two Gaussian components of Hβ were free to vary.

The final spectra, best-fit model, and model components are plotted in Figures 1–3. These fits are the ones used for the FWHM (Hβ) listed in Table 2. The final FWHM of the entire Hβ profile was measured, as well as the FWHM of the [O iii] lines. We estimated the uncertainty on the width of the lines by slightly shifting the parameters from their best-fit values and marking the most extreme values that would still represent a reasonable fit to the Hβ complex. In almost all of the cases, those uncertainties were smaller than the instrumental resolution ($\sim$600 km s^{-1}) for the TNG and AAT spectra, with UM 645, [HB89] 2254+024, 2QZ J002830.4−281706, and 2QZ J231456.8−280302 being the only exceptions (see Figs. 1–3).

We have also obtained direct measures of the fluxes and FWHMs of Hβ and [O iii] by integrating across the Fe ii–subtracted features, for the flux measurements, and by taking the width at half the peak value for each Fe ii–subtracted feature, in the FWHM measurements. Both types of measurements, the best-fit value and the "direct" feature method, appear in Table 2 and Paper II. The difference between both methods can be regarded as an estimate of the uncertainty of those measurements, although these are not pure statistical errors. This paper presents the Hβ line width for our sources. Other line properties, and in particular those of [O iii] and Fe ii, are discussed in Paper II.

It is expected that each Hβ profile in our $2 < z < 3.5$ sample is a blend of a narrow component, emitted from the narrow-line region (NLR), and a broad BLR component, which we will use to determine $M_{\rm BH}$. Resolving each of those two physical components can be done if there is an obvious NLR spike in the Hβ profile, as is the case for several broad-line Seyfert 1 galaxies (BLS1s). In cases where a narrow spike is undetected, the NLR contribution to the Hβ emission can in principal be estimated by taking FWHM ([O iii] λ5007) as its width and

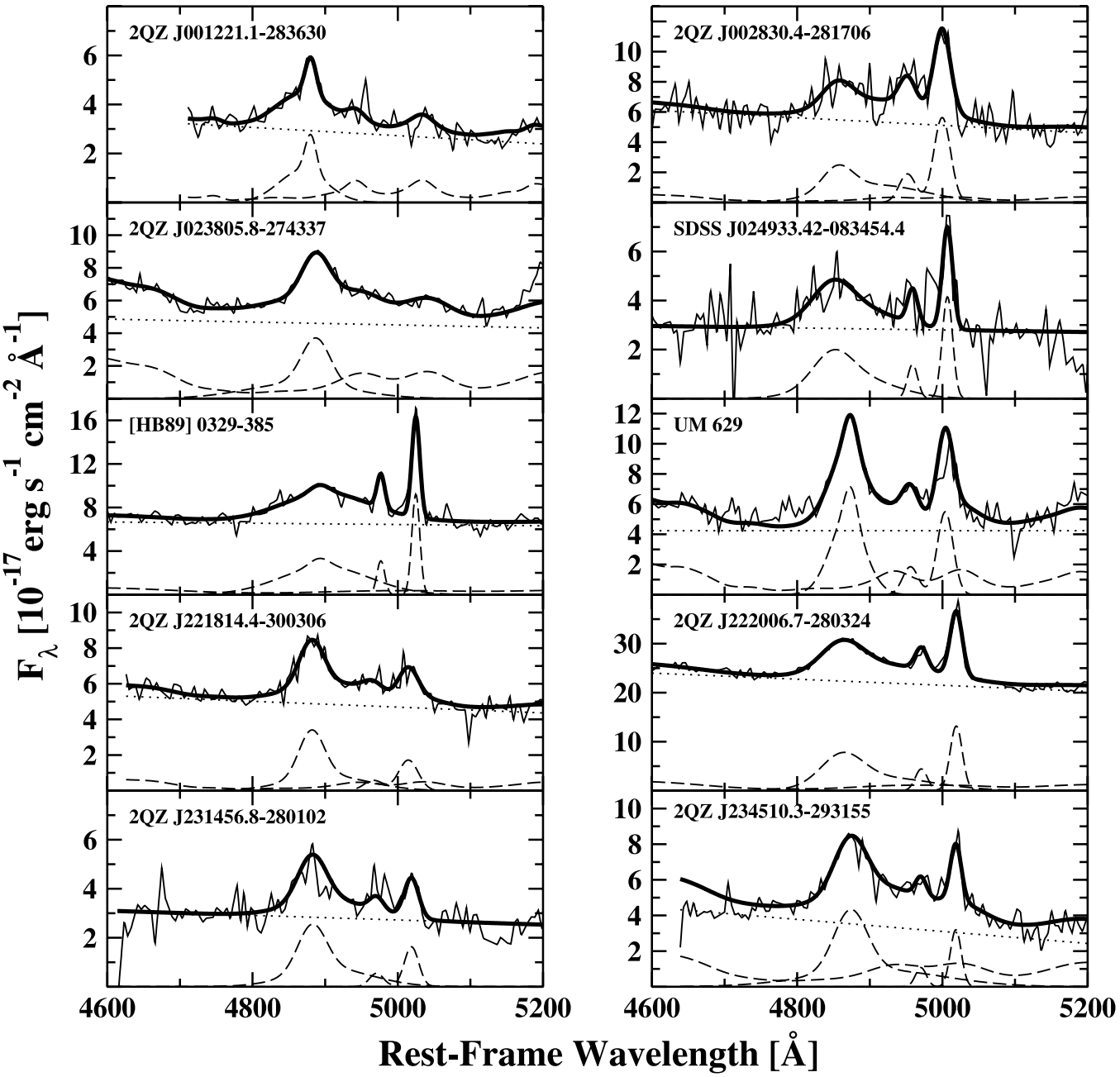

FIG. 1.—IR spectra of $2 < z < 2.5$ quasars obtained at AAT. The spectrum in each panel is represented by a thin solid line. The model (*thick line*) is composed of a continuum (*dotted line*), Fe II emission, Hβ, and [O III] (*long-dashed lines*).

by taking its flux as a certain fraction of the [O III] λ5007 flux. This method is highly model-dependent, and in many of our sources we do not detect [O III] emission at all (see Paper II). The two Gaussians we fitted to Hβ do not attempt to recover the *physical* NLR and BLR components, but merely to represent a fit to the entire profile. In luminous AGNs the NLR-to-BLR flux ratio, at least in the UV lines, is of the order of a few percent (e.g., Wills et al. 1993), resulting in a negligible NLR contribution to the line flux. Since we also do not detect a significant NLR spike *in any* of our Hβ profiles, we assume that the observed line represents entirely the BLR contribution.

We have also obtained another measure of line width, based on the entire emission-line flux, regardless of the profile. This is the interpercentile velocity (IPV) width, which we have used for measuring the difference between wavelengths corresponding to 25% and 75% of the integrated emission-line flux across the entire line profile, starting with the continuum on the blue side and ending with the continuum on the red side of the line. Both the FWHM and IPV methods have their own merits, although it is still not clear which gives the closest estimate of the BLR velocity width (see Corbett et al. 2003 and references therein). In most cases, the IPV widths of Hβ are somewhat narrower than the corresponding FWHM (by $\sim$15%; for a Gaussian profile the IPV width should be $\sim$43% narrower than the corresponding FWHM), although both methods give consistent line widths within the uncertainties discussed above.

3.2. *Luminosity, BH Mass, and Accretion Rate*

We have derived monochromatic luminosities for our entire AGN sample at the rest-frame 5100 Å band using our new IR

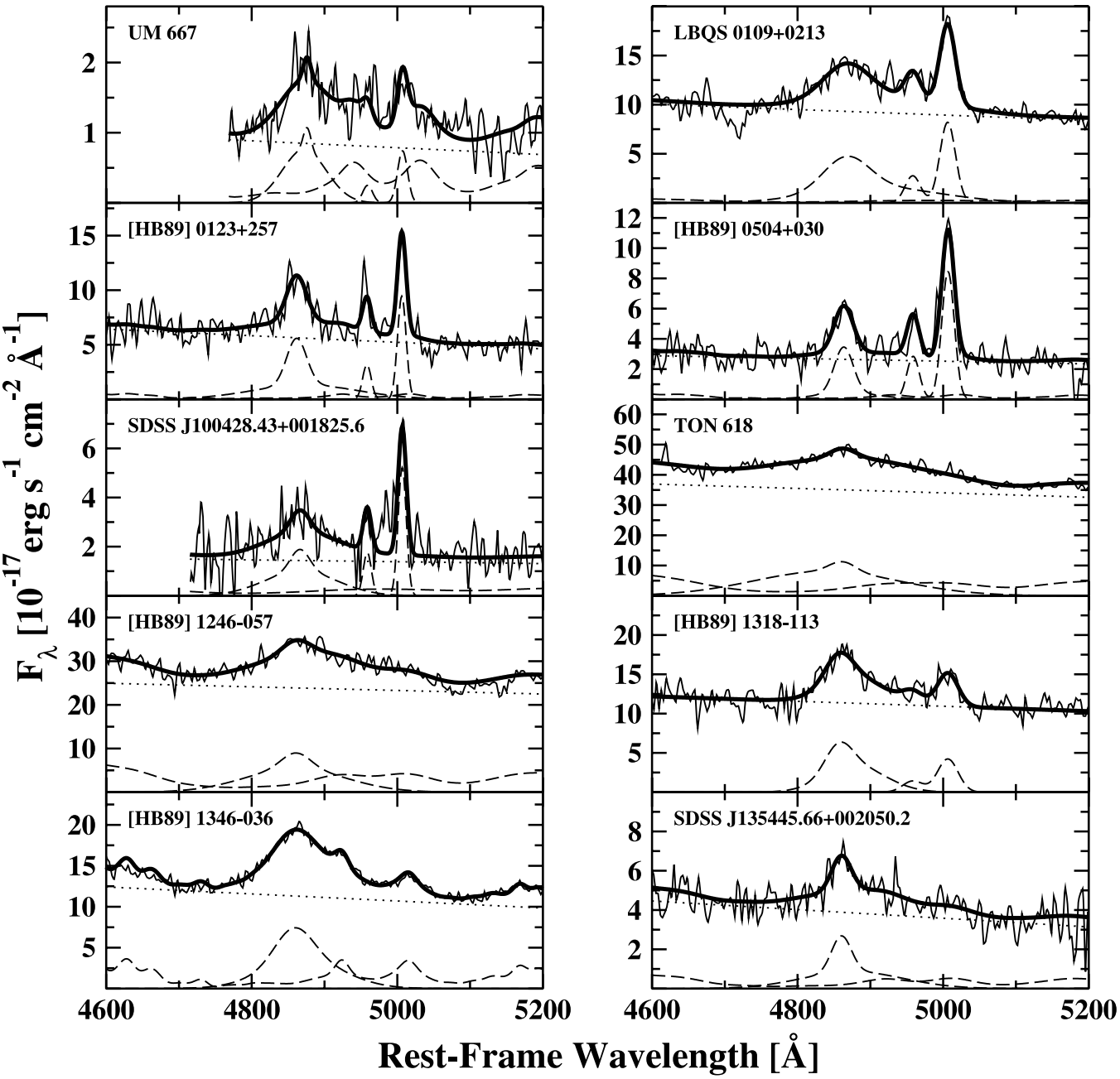

FIG. 2.—IR spectra of $2 < z < 3.5$ quasars obtained at TNG. Symbols are the same as in Fig. 1.

observations and data from the literature and compared them with the monochromatic luminosities at the rest-frame 1450 Å band obtained from the literature and from the archives of the SDSS and the Two-Degree Field (2dF) quasar redshift survey (2QZ; Croom et al. 2004). For 10 sources we could not find 5100 Å fluxes, including six sources from our high-z sample (see Table 1). In those cases we obtained the 5100 Å luminosity by extrapolating from 1450 Å fluxes and assuming (as explained in § 2) a continuum function of the form $f_\nu \propto \nu^{-0.5}$. Figure 4 shows this comparison, along with two lines indicating a 1:1 correspondence and 1:$(5100/1450)^{1/2}$, representing the expected ratio between the 1450 and the 5100 Å bands for a $f_\nu \propto \nu^{-\alpha}$ continuum with $\alpha = 0.5$. Most AGNs lie between the two lines, indicating perhaps a somewhat redder ($\alpha > 0.5$) continuum for our sample. We also note that most RLQs in our sample are slightly redder than the radio-quiet objects, consistent with the steep continuum slopes in RLQs found by Netzer et al. (1995). Since the luminosities in both bands are highly correlated, and in order to avoid complications due to intrinsic reddening, we prefer to use the 5100 Å luminosities[8] over the 1450 Å luminosities in determining BH masses and accretion rates in our entire sample.

Black hole masses and accretion rates were determined by the single-epoch mass determination method (Vestergaard 2002), which is based on the Kaspi et al. (2000, hereafter K00) $R_{\rm BLR} - \lambda L_\lambda(5100)$ correlation, where $\lambda L_\lambda(5100)$ is the

[8] For a few nearby Seyfert 1 galaxies in our sample, this choice might add contamination from the host galaxy. However, in most cases such a contribution is much less than 50%, which is an acceptable uncertainty level, given the typical large expected continuum variations.

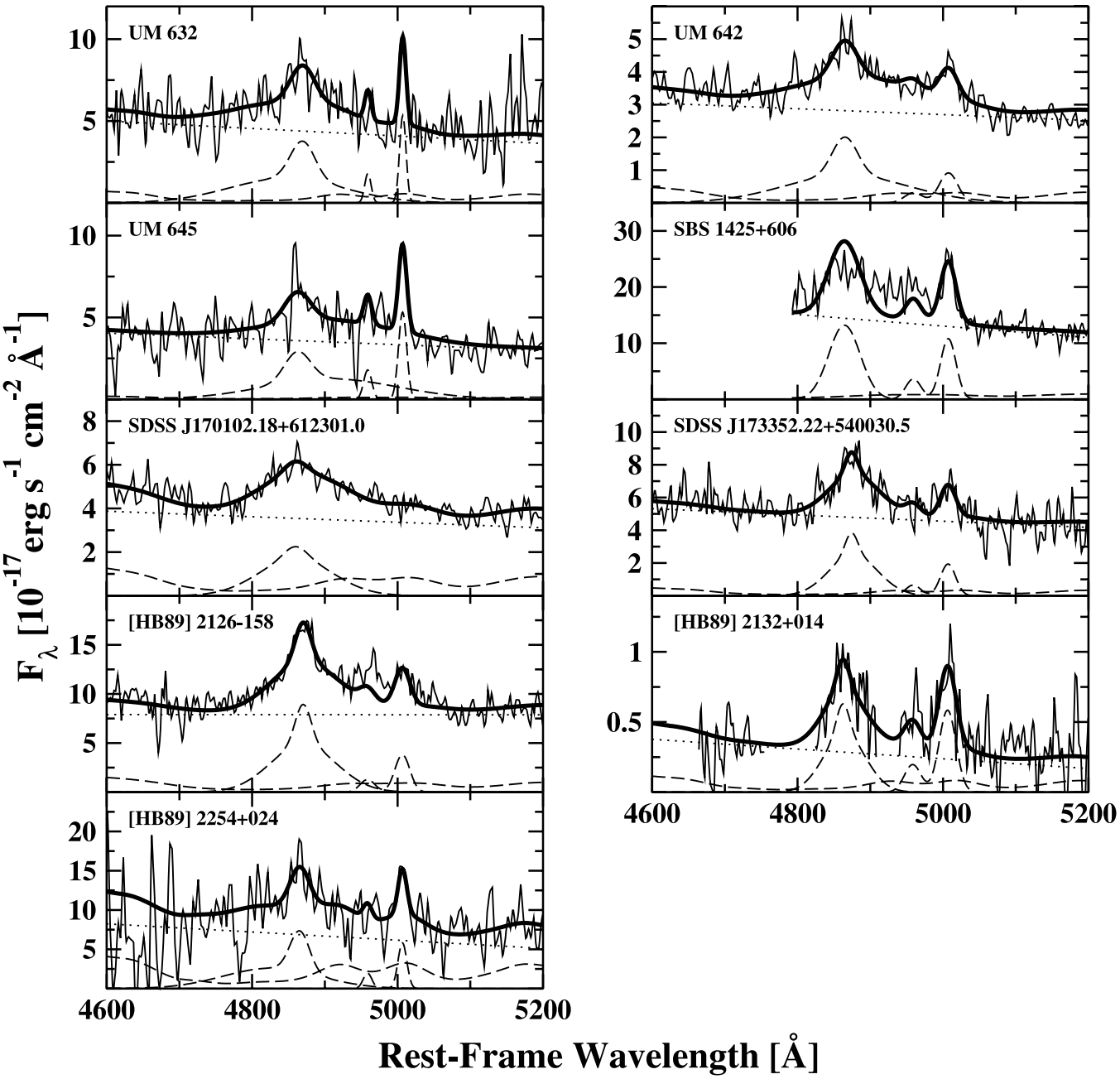

FIG. 3.—IR spectra of $2 < z < 3.5$ quasars obtained at TNG (*continued*). Symbols are the same as in Fig. 2.

monochromatic luminosity at 5100 Å. In this method the BLR size is estimated from the measured $\lambda L_\lambda(5100)$, and the mass estimate follows from assuming Keplerian motion of the Hβ-emitting gas. The scaling used here is based on a reanalysis of the K00 measurements (Peterson et al. 2004; S. Kaspi et al. 2004, in preparation) that gives $R_{\rm BLR} \propto \lambda L_\lambda(5100)^{0.6}$ with a somewhat different size scaling factor. It also uses a somewhat different mass scaling factor that multiplies the FWHM (Hβ) term in the mass determination equation (see K00). The result,

$$M_{\rm BH} = 6.2\times10^6 \left[\frac{\lambda L_\lambda(5100)}{10^{44}\ {\rm ergs\ s^{-1}}}\right]^{0.6} \left[\frac{\rm FWHM\,(H\beta)}{10^3\ {\rm km\ s^{-1}}}\right]^2 M_\odot, \quad (1)$$

gives slightly larger masses compared with K00 and Netzer (2003). We then convert the observed luminosity and the deduced masses to accretion rates, represented by $L_{\rm Bol}/L_{\rm Edd}$, by assuming $L_{\rm Bol} = 7\times\lambda L_\lambda(5100)$. The factor of 7 is in the middle of the range (5–9) representing observed and theoretically deduced spectral energy distributions (SEDs; see Netzer 2003). The result is

$$L_{\rm Bol}/L_{\rm Edd} = 0.75 \left[\frac{\lambda L_\lambda(5100)}{10^{44}\ {\rm ergs\ s^{-1}}}\right]^{0.4} \left[\frac{\rm FWHM\,(H\beta)}{10^3\ {\rm km\ s^{-1}}}\right]^{-2}. \quad (2)$$

Table 2 lists luminosity, $M_{\rm BH}$, and $L_{\rm Bol}/L_{\rm Edd}$ (hereafter $L/L_{\rm Edd}$) for our new $2 < z < 3.5$ quasars. By combining the measurement uncertainties on FWHM (Hβ), as given in Table 2 and discussed in § 3.1, with the small ($\sim$25%) uncertainty on the luminosity, we obtain typical uncertainties on $M_{\rm BH}$ and on $L/L_{\rm Edd}$, which are not larger than a factor of 2 and therefore do not affect our main results as outlined below.

TABLE 2
Emission Line and Continuum Measurements

Quasar Name	$\log \lambda L_\lambda(5100)$ (ergs s^{-1})	FWHM (Hβ) Best Fit (km s^{-1})	FWHM (Hβ) Direct (km s^{-1})	$\log M_{BH}$ ($M_\odot$)	L/L_{Edd}	N v/C iv	Reference for UV Data
2QZ J001221.1−283630	46.26	1915	2382	8.71	1.64	0.84	1
2QZ J002830.4−281706	46.58	4833	5295	9.71	0.35	0.47	1
UM 667	46.28	3135	2244	9.15	0.62	0.81	2
LBQS 0109+0213	46.80	5781	5241	10.00	0.30	0.82	3
[HB89] 0123+257	46.57	2406	2763	9.09	1.38	0.77	2
2QZ J023805.8−274337	46.57	3437	3691	9.40	0.68	0.90	1
SDSS J024933.42−083454.4	46.38	5230	6601	9.66	0.25	1.07	4
[HB89] 0329−385	46.71	7035	8165	10.11	0.18	0.86	5
[HB89] 0504+030	46.32	2046	2402	8.80	1.52	0.48	6
SDSS J100428.43+001825.6	46.44	3442	3586	9.33	0.60	1.53	7
TON 618	47.31	10527	14905	10.82	0.14	1.60	8
[HB89] 1246−057	47.16	5817	6842	10.22	0.41	1.82	5
[HB89] 1318−113	46.89	4150	4898	9.75	0.61	0.56	5
[HB89] 1346−036	46.88	5110	5129	9.94	0.41	0.78	5
SDSS J135445.66+002050.2	46.49	2627	2208	9.13	1.08	2.93	7
UM 629	46.56	2621	2521	9.16	1.15	0.80	7
UM 632	46.54	3614	3828	9.43	0.60	0.28	6
UM 642	46.29	3925	5478	9.35	0.40	0.51	7
UM 645	46.31	3966	4972	9.37	0.40	0.29	7
SBS 1425+606	47.38	3144	6769	9.82	1.71	0.47	2
SDSS J170102.18+612301.0	46.34	5760	5944	9.72	0.20	1.19	7
SDSS J173352.22+540030.5	47.00	3078	5460	9.57	1.26	1.79	7
[HB89] 2126−158	47.25	3078	3354	9.72	1.58	0.77	2
[HB89] 2132+014	45.77	2505	2801	8.65	0.61	0.80	2
2QZ J221814.4−300306	46.54	2986	3070	9.27	0.88	0.96	1
2QZ J222006.7−280324	47.22	5238	5660	10.16	0.53	1.67	1
[HB89] 2254+024	46.45	2597	1954	9.09	1.07	0.59	6
2QZ J231456.8−280102	46.31	3459	2011	9.26	0.53	1.21	1
2QZ J234510.3−293155	46.32	3908	3453	9.37	0.42	1.59	1

References.—(1) 2QZ archive (Croom et al. 2004); (2) Dietrich & Wilhelm-Erkens 2000; (3) Forster et al. 2001; (4) SDSS first data release (Abazajian et al. 2003); (5) Osmer & Smith 1977; (6) Baldwin et al. 1989; (7) SDSS early data release (Stoughton et al. 2002); (8) Baldwin & Netzer 1978.

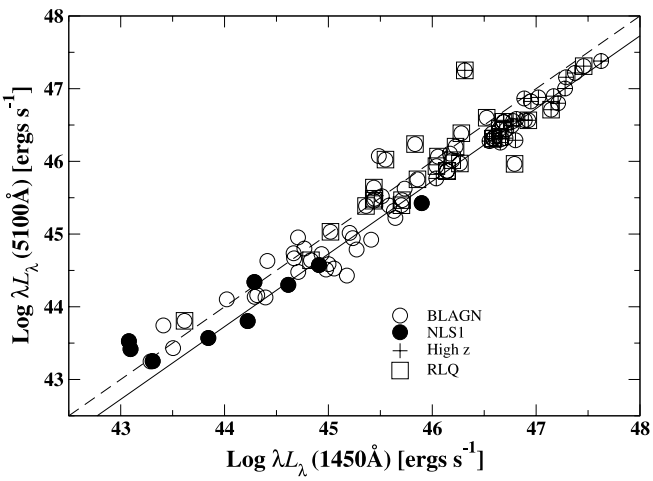

Fig. 4.—Monochromatic luminosities at 5100 vs. 1450 Å for the sample of 92 AGNs. Empty circles are broad-line AGNs (BLAGNs) with FWHM (Hβ) > 1500 km s^{-1}, and empty circles with plus signs indicate $2 < z < 3.5$ quasars. NLS1s [with FWHM (Hβ) < 1500 km s^{-1}; see SN02] are marked with filled circles, and RLQs are marked with empty squares. The dashed line marks a 1:1 correspondence, and the solid line marks an empirical ratio of $\lambda L_\lambda(1450)/\lambda L_\lambda(5100) = [(5100/1450)]^{1/2}$ assuming $f_\nu \propto \nu^{-\alpha}$ with $\alpha = 0.5$. Most AGNs lie closer to the dashed line, indicating somewhat larger α.

A similar determination of M_{BH} and L/L_{Edd} was applied to LBQS 0256−0019, LBQS 0302−0000, and the 61 sources from the SN02 sample. It is worth noting at this point that, within our new (albeit small) sample of luminous high-z quasars, there is no clear relation between M_{BH} and radio loudness (see Tables 1 and 2), as was previously suggested in several studies, e.g., Franceschini et al. (1998), and it is therefore consistent with the results of Woo & Urry (2002).

3.3. *BLR Metallicity*

Following HF93, we use N v/C iv as the BLR metallicity indicator for our sample. This line ratio is easier to measure than most other emission lines in a typical spectrum and was considered by Hamann et al. (2002) as a robust indicator since it minimizes nonabundance effects, such as temperature, and SED. About half of our quasars have rest-frame UV data available in the literature, and we complemented these data with measurements of N v and C iv for the rest of the sample, which are mostly recently detected quasars. Rest-frame UV spectra of those sources were obtained from the SDSS and 2QZ archives. The standard SDSS data allow reasonably accurate flux calibration and SED determination. The shape of the non–flux-calibrated 2QZ spectra is more problematic and was obtained by dividing each spectrum by a quadratic, which provides a reasonable estimate of the spectral response function of the 2dF (Folkes et al. 1999). Each SDSS and 2QZ

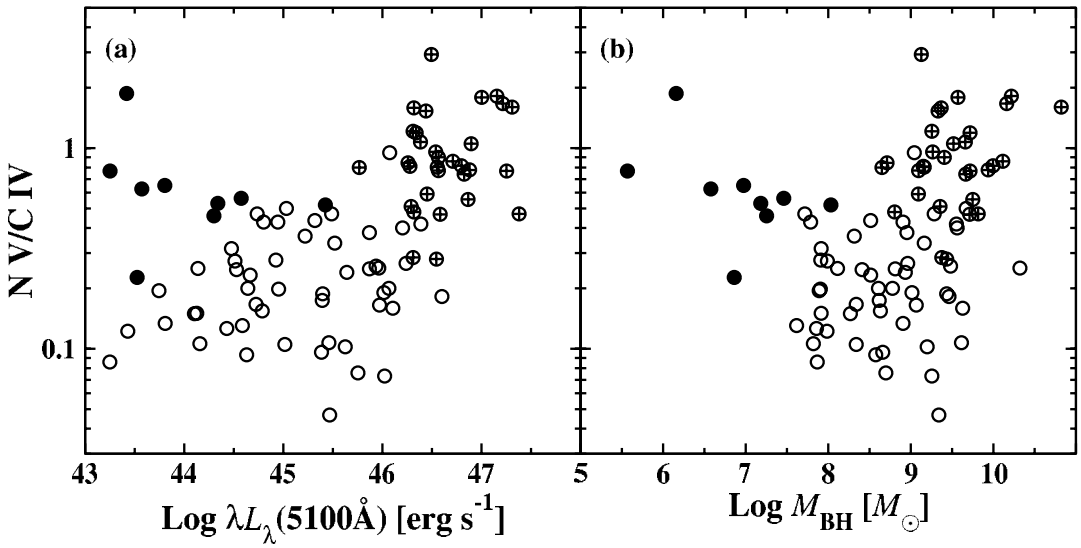

FIG. 5.—N v/C iv vs. (*a*) luminosity and (*b*) M_{BH}. Symbols are the same as in Fig. 4. NLS1s clearly lie away from the trend followed by the BLAGNs and our high-*z* quasars.

spectrum was fitted with a power-law continuum, and two Gaussians for the C iv emission line. The C iv profile was then used as a template for all other rest-frame UV emission lines, and in particular N v. We list N v/C iv measurements for our 29 $2 < z < 3.5$ quasars in Table 2. The uncertainties on the measurement of this ratio vary between ~10% for the high-quality spectra and ~30% for the poorer quality ones (see also SN02).

4. RESULTS

4.1. *A New Metallicity–Accretion Rate Relationship in AGNs*

In Figure 5 we plot N v/C iv versus (*a*) $\lambda L_\lambda(5100)$ and (*b*) M_{BH} for our sample of 92 AGNs. One can see that the *Z-L* and *Z-*M_{BH} relations show considerable scatter, mainly due to the NLS1s, which have low BH masses and luminosities. The first of those relations has been shown and discussed by SN02 for a slightly larger sample. The scatter is significantly reduced once metallicity is plotted against accretion rate as shown in Figure 6. In this case, *all* AGNs follow a strong metallicity–accretion rate (N v/C iv–L/L_{Edd}; hereafter *Z-*L/L_{Edd}) correlation with NLS1s *being no exception*.

Table 3 lists the Spearman rank correlation coefficients (r_S) and the chance probabilities (P) for each of the three relations. We also tested the correlations by removing the 10 NLS1s from the sample. As can be seen from Table 3, this increases r_S considerably in the *Z-L* and *Z-*M_{BH} cases, but their removal from the *Z-*L/L_{Edd} diagram leaves r_S almost unchanged. We note that, formally, both the *Z-L* and the *Z-*M_{BH} correlations are significant ($P \ll 0.01$). This represents the fact that our sample contains only 10 NLS1s out of 92 sources (representing well their fraction in the AGN population). However, this subgroup clearly lies away from the general trend in Figures 5*a* and 5*b*, emphasizing the fact that they do not share the same properties with other low-luminosity/M_{BH} AGNs.

To summarize, our results indicate that the N v/C iv line ratio is correlated primarily with L/L_{Edd} and not with luminosity or BH mass. It is the combination of luminosity *and* line width (i.e., the accretion rate) that makes all the AGNs in our sample, including NLS1s, follow the same trend. We caution that our entire sample of 92 AGNs is neither complete nor fully representative of the AGN population as a whole, and that our main result may be subject to selection biases over the wide range of AGN properties, which were not fully explored in this work.

4.2. FWHM (Hβ) *versus* FWHM (C iv) *as Accretion Rate Indicators*

Reverberation BH masses were so far determined for 35 AGNs using Hβ and the monochromatic luminosity at 5100 Å (K00; Peterson et al. 2004) to set the empirical *R-L* relation on which all M_{BH} estimates are made. For three AGNs, reverberation masses were also determined using C iv (Peterson & Wandel 2000) and were consistent with the masses obtained from Hβ. Vestergaard (2002) suggested that C iv can be used as a "proxy" to Hβ and replace it as the reverberation M_{BH} indicator. It is expected that the BLR components of both lines

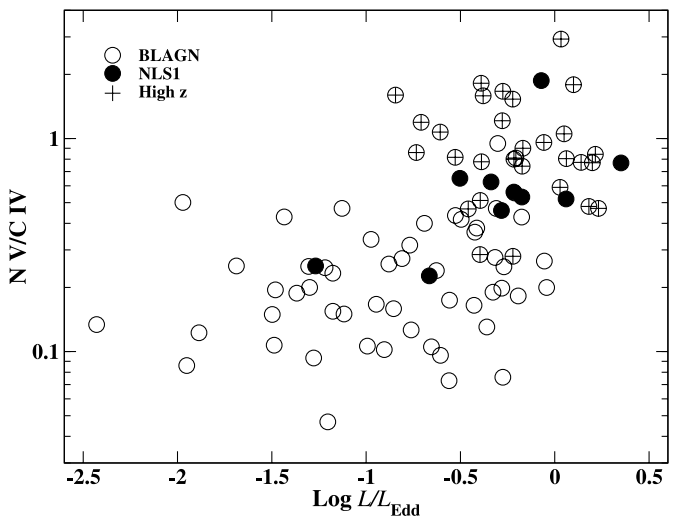

FIG. 6.—N v/C iv vs. accretion rate. Symbols are similar to those in Fig. 4. A strong metallicity-accretion rate correlation *for all AGNs* is apparent, and most NLS1s are found in the same region of parameter space that is shared by the high-*z* quasars. Note that the location of Mrk 766 (the NLS1 with the lowest accretion rate in this diagram) may be affected by strong intrinsic reddening (see text).

TABLE 3
Spearman Rank Correlation Coefficients

N V/C IV versus	Number of Sources	r_S	P
L/L_{Edd}[a]	92	0.57	$<10^{-5}$
L/L_{Edd}[a]	82[b]	0.54	$<10^{-5}$
M_{BH}[a]	92	0.35	3.1×10^{-4}
M_{BH}[a]	82[b]	0.53	$<10^{-5}$
$\lambda L_\lambda(5100)$	92	0.53	$<10^{-5}$
$\lambda L_\lambda(5100)$	82[b]	0.71	$<10^{-5}$
L/L_{Edd}[c]	82	0.32	1.6×10^{-3}
L/L_{Edd}[c]	72[b]	0.41	1.7×10^{-4}

[a] Calculated from $\lambda L_\lambda(5100)$ and FWHM (Hβ).
[b] NLS1s excluded.
[c] Calculated from $\lambda L_\lambda(1450)$ and FWHM (C IV).

will satisfy FWHM (C IV)/FWHM (Hβ) $\simeq \sqrt{2}$, based on reverberation studies of both lines that show a smaller mean emission distance for C IV (Peterson & Wandel 2000).

We have measurements of both Hβ and C IV in 82 AGNs of our sample, and the width of one line versus the width of the other is plotted in Figure 7. One can clearly see that the widths of both lines do not follow a 1:1 correspondence nor a $1:\sqrt{2}$ dependence. In particular, NLS1s with narrow Hβ lines show FWHM (C IV), which is not different from those of "normal" BLS1s, a fact that was first noted by Rodriguez-Pascual et al. (1997). Broad C IV in NLS1s, and in other AGNs, has been attributed to high-velocity gas outflowing from the center rendering a broad and blueshifted tail to this line (e.g., Leighly 2000).

To demonstrate the influence of FWHM (C IV) on NLS1 M_{BH} estimates, we compared the Vestergaard (2002) single-epoch M_{BH} estimated from the UV spectrum with the reverberation M_{BH} from K00, directly measured from the Hβ width, for four NLS1s. We find that, on average, the M_{BH} UV estimates are larger by a factor of $\sim$3 than the M_{BH} measured by optical reverberation mapping. Hence, M_{BH} calculated from C IV, at least for NLS1s, may be systematically higher than M_{BH} estimates using Hβ. An opposite behavior is also apparent in Figure 7, namely narrow C IV for broad Hβ.

To further illustrate the problematic use of C IV for individual sources, we recalculated the BH mass and accretion rate, this time using the width of C IV, together with the Vestergaard (2002) R_{BLR}-L relation. Figure 8 plots N V/C IV versus accretion rate, and Table 3 lists the corresponding Spearman rank correlation coefficients. By inspection of Figure 8 and Table 3 it is apparent that the correlation between the accretion rate calculated from the C IV width and N V/C IV is much weaker compared with the accretion rate calculated from Hβ, and that the Z-L/L_{Edd} now has much more scatter. This result may also explain the lack of a Z-L/L_{Edd} correlation in Warner et al. (2004).

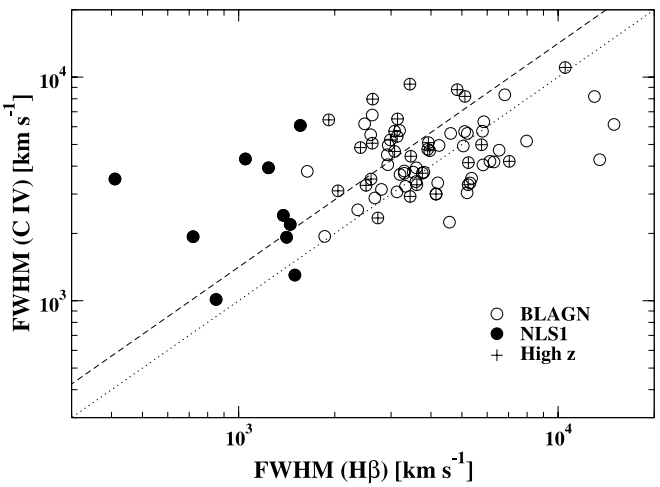

Fig. 7.—FWHM (C IV) vs. FWHM (Hβ) for 82 objects in our entire sample. Symbols are similar to those in Fig. 6. Dotted (dashed) lines represent a 1:1 ($1:\sqrt{2}$) relation, respectively.

5. DISCUSSION

The main result presented in this paper is a strong correlation between metallicity (á la HF93) and accretion rate in a sample of 92 AGNs spanning a broad range of AGN luminosity ($\sim 10^{42}$–10^{48} ergs s^{-1}), line width, and radio loudness. We also confirm the earlier SN02 finding that AGN samples that include NLS1s do not show a clear Z-L correlation. The new relationship, although supported by a strong correlation, is not free of scatter, and the effects of other physical properties are still unknown. In this section we discuss potential sources for intrinsic scatter in the Z-L/L_{Edd} diagram as well as potential caveats in the derivation of BLR metallicity and accretion rate. We also comment on the potential implications of our new result for metal enrichment and BH growth scenarios in galactic nuclei and for the starburst-AGN connection.

5.1. *How Accurate is the BH Mass Determination at High Luminosity?*

Our estimates of BH mass, and hence accretion rate, rely on the K00 relationship applied to a sample of 34 AGNs with BH masses measured via reverberation mapping and modified, slightly, in S. Kaspi et al. (2004, in preparation). That relationship is limited by the small number of sources, the luminosity range ($\sim 10^{42}$–10^{45}), the assumed constant SED, and perhaps other AGN properties. Mass estimates for sources beyond this luminosity range are therefore uncertain. Such extrapolations lead to BH masses exceeding $10^{10}\,M_\odot$ in this work and in Netzer (2003). Hence, if we have somewhat overestimated M_{BH} in our luminous AGN sample, then the accretion

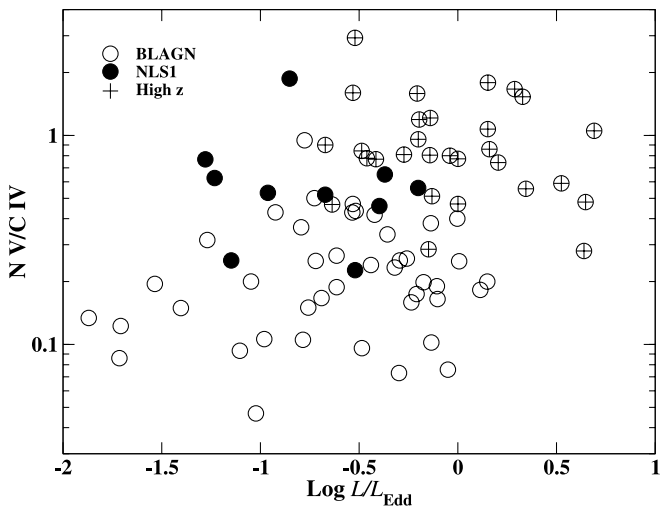

Fig. 8.—N V/C IV vs. accretion rate determined from a combination of $\lambda L_\lambda(1450)$ and FWHM (C IV). Symbols are similar to those in Fig. 6. Note the considerable scatter, compared with Fig. 6, as a consequence of using C IV as an accretion rate indicator.

rate must have been underestimated. This will move luminous quasars to the right-hand side of Figure 6 and will produce an even stronger Z-$L/L_{\rm Edd}$ correlation. However, a very different L-$M_{\rm BH}$ relationship at high luminosity may introduce more scatter into some of the correlations presented here.

5.2. *Is* N v/C iv *an Adequate Metallicity Indicator for all AGNs?*

Using a grid of photoionization calculations, performed with the locally optimally emitting cloud model (LOC; e.g., Baldwin et al. 1995), Hamann et al. (2002) found that N v/C iv can trace the BLR gas metallicity, and it only weakly depends on the chosen SED and density. Our new results show that N v/C iv depends primarily on $L/L_{\rm Edd}$, but it is not yet clear whether high N v/C iv is indeed indicative of high metallicities. In particular, it is crucial to compare the observations of this line ratio to those of the model-independent weak lines proposed by Shields (1976). Our investigation of this issue is beyond the scope of this work (see also Dietrich et al. 2003).

Part of the scatter in the Z-$L/L_{\rm Edd}$ diagram may be contributed by the yet unknown effect of BLR density on the way BLR metallicity is derived. The problem has been mentioned by HF93, but the observational verification is still missing. It is reasonable to assume that high metal contents are associated with high densities in the nuclear region, which are indicators of recent star formation. In particular, NLS1s, which have high ratios of N v/C iv, are also known to have high BLR densities, derived from the Si iii] λ1892/C iii] λ1909 density-sensitive line ratio (e.g., Wills et al. 1999). We have measured this line ratio in our sample (available for about half of our sources) and found no clear trend with either metallicity or accretion rate. The two emission lines used for this ratio, which are fairly close to each other, are hard to measure and to deblend. Therefore, the potential effect of the BLR density remains unclear at this stage.

The continuum SED may also affect the way N v/C iv depends on BLR metallicity. It is not yet clear whether the SED depends on luminosity, or perhaps the accretion rate, but if the SED in high accretion rate sources is significantly different from the ones used by Hamann et al. (2002) to calculate N v/C iv, then it may cause some deviation from the canonical Z-L dependence. In particular, NLS1s appear to have SEDs that are somewhat different from "standard" AGN SEDs (e.g., Romano et al. 2004) and related perhaps to the putative (hotter) slim accretion disk (e.g., Wang & Netzer 2003). As explained in § 3.2, a different SED may also affect our derived $L/L_{\rm Edd}$.

A viable model of AGN evolution is that they start off with high accretion rates when fuel supply is abundant and gradually move toward lower accretion rates as the fuel supply dwindles. If the metal content of the gas does not change as a consequence of the fuel shortage, one can expect an AGN to move horizontally, from right to left, across the Z-$L/L_{\rm Edd}$ diagram (Fig. 6) as a function of time. In other words, similar metallicities may be observed for a range of accretion rates. The dependence on age may be further complicated by the AGN duty cycle (assumed to be $\sim 10^7$–10^8 yr), as we do not know the number of cycles each AGN in our sample has gone through. If metal enrichment is strongly related to AGN fueling, then a number of active episodes may contribute to metal enrichment provided the metal-rich gas is not being depleted or blown out of the nucleus. This can lead to a Z-$L/L_{\rm Edd}$ dependence that is more complicated than the one assumed here.

5.3. *Intrinsic Reddening*

Intrinsic reddening may affect the location of an AGN on the Z-$L/L_{\rm Edd}$ diagram by moving it diagonally toward the bottom left corner in Figure 6, as a result of weaker N v with respect to C iv and lower luminosity. Correcting for intrinsic reddening is problematic and requires a broader spectral range to compare suitable line ratios (e.g., Crenshaw et al. 2002). We did not attempt to correct the data for intrinsic reddening but note that in the case of NLS1s such a correction may be necessary, since these objects are suspected of possessing large amounts of dust and gas (e.g., Crenshaw et al. 2003). We note that at least one NLS1 in our sample (Mrk 766) may be strongly affected by intrinsic reddening, which might explain its location in Figure 6, away from the rest of the NLS1 population.

5.4. *Metal Enrichment and BH Growth in Galactic Centers*

If N v/C iv is an adequate BLR metallicity indicator, then our Z-$L/L_{\rm Edd}$ correlation may have important implications for the understanding of BH growth in galactic nuclei as well as for the starburst-AGN connection. We find that luminous quasars at high redshift, as well as NLS1s in the nearby universe, may be experiencing (or have recently experienced) a vigorous star-forming episode and that their BHs are in the stage of rapid growth. In this sense, the NLS1s in our sample may be in the early stages of their (current) activity, i.e., relatively "young" systems, as suggested by Mathur (2000). All the high-z quasars in our sample also exhibit high accretion rates and high metallicities and may be in a similar evolutionary stage. These sources are thus the high-luminosity analogs of NLS1s and should perhaps be referred to as narrow-line type 1 quasars (NLQ1s). However, our sample does not contain faint quasars at large distances, and those must be added to the sample to test this idea. In particular, our new Z-$L/L_{\rm Edd}$ relationship may be affected by a potential selection effect against low accretion rate AGNs at high z, if such sources are found to be metal-rich. Our new result is consistent with a scenario in which there is an intimate relation between AGN fueling, manifested by accretion rate, and starburst, responsible for the metal enrichment. An obvious avenue to take is to search for other evidence of recent star formation in our high-z sample using IR, millimeter, and submillimeter observations.

6. CONCLUSIONS

We present new near-IR spectroscopic measurements of the Hβ region for a sample of 29 luminous $2 < z < 3.5$ quasars. This sample is augmented with measurements of other AGNs (92 AGNs in total) for which spectroscopic data of the rest-frame UV band as well as the Hβ region are available. We show that BLR metallicity, indicated by N v/C iv, is primarily correlated with the accretion rate, indicated by luminosity and FWHM (Hβ). We also show that using C iv as a proxy to Hβ may be problematic and can lead to spurious BH mass estimates. The potential implications of our new result for the starburst-AGN connection and for AGN fueling are briefly discussed.

We are grateful to the technical staff at the Anglo-Australian Telescope (AAT) and Italian Telescopio Nazionale Galileo (TNG) observatories for invaluable help during the observations. This work is based on observations made with TNG

operated on the island of La Palma by the Centro Galileo Galilei of the Istituto Nazionale di Astrofisica (INAF) at the Spanish Observatorio del Roque de los Muchachos of the Instituto de Astrofisica de Canarias. We would like to thank Angela Cotera for allowing us to use half a night of her time at AAT, and Dirk Grupe for providing us an electronic version of the Boroson & Green (1992) Fe II template. We gratefully acknowledge constructive remarks from an anonymous referee, who helped to improve this work considerably. The Two-Degree Field QSO Redshift Survey (2QZ) was compiled by the 2QZ survey team from observations made with the Two-Degree Field on the AAT. Funding for the creation and distribution of the SDSS Archive has been provided by the Alfred P. Sloan Foundation, the Participating Institutions, the National Aeronautics and Space Administration, the National Science Foundation, the US Department of Energy, the Japanese Monbukagakusho, and the Max Planck Society. The SDSS Web site is http://www.sdss.org. The SDSS is managed by the Astrophysical Research Consortium (ARC) for the Participating Institutions. The Participating Institutions are the University of Chicago, Fermilab, the Institute for Advanced Study, the Japan Participation Group, the Johns Hopkins University, Los Alamos National Laboratory, the Max-Planck-Institute for Astronomy (MPIA), the Max-Planck-Institute for Astrophysics (MPA), New Mexico State University, University of Pittsburgh, Princeton University, the United States Naval Observatory, and the University of Washington. This research has made use of the NED database, which is operated by the Jet Propulsion Laboratory, California Institute of Technology, under contract with the National Aeronautics and Space Administration. This work is supported by Israel Science Foundation grant 232/03. R. M. acknowledges partial support by the Italian Ministry of Research (MIUR).

REFERENCES

Abazajian, K., et al. 2003, AJ, 126, 2081
Baldwin, J., Ferland, G., Korista, K., & Verner, D. 1995, ApJ, 455, L119
Baldwin, J. A., & Netzer, H. 1978, ApJ, 226, 1
Baldwin, J. A., Wampler, E. J., & Gaskell, C. M. 1989, ApJ, 338, 630
Boroson, T. A., & Green, R. F. 1992, ApJS, 80, 109
Corbett, E. A., et al. 2003, MNRAS, 343, 705
Crenshaw, D. M., Kraemer, S. B., & Gabel, J. R. 2003, AJ, 126, 1690
Crenshaw, D. M., et al. 2002, ApJ, 566, 187
Croom, S. M., Smith, R. J., Boyle, B. J., Shanks, T., Miller, L., Outram, P. J., & Loaring, N. S. 2004, MNRAS, 349, 1397
Dietrich, M., Appenzeller, I., Vestergaard, M., & Wagner, S. J. 2002, ApJ, 564, 581
Dietrich, M., Hamann, F., Shields, J. C., Constantin, A., Heidt, J., Jäger, K., Vestergaard, M., & Wagner, S. J. 2003, ApJ, 589, 722
Dietrich, M., & Wilhelm-Erkens, U. 2000, A&A, 354, 17
Folkes, S., et al. 1999, MNRAS, 308, 459
Forster, K., Green, P. J., Aldcroft, T. L., Vestergaard, M., Foltz, C. B., & Hewett, P. C. 2001, ApJS, 134, 35
Franceschini, A., Vercellone, S., & Fabian, A. C. 1998, MNRAS, 297, 817
Hamann, F., & Ferland, G. 1993, ApJ, 418, 11
Hamann, F., Korista, K. T., Ferland, G. J., Warner, C., & Baldwin, J. 2002, ApJ, 564, 592
Kaspi, S., Smith, P. S., Netzer, H., Maoz, D., Jannuzi, B. T., & Giveon, U. 2000, ApJ, 533, 631
Kellermann, K. I., Sramek, R., Schmidt, M., Shaffer, D. B., & Green, R. 1989, AJ, 98, 1195
Lançon, A., & Rocca-Volmerange, B. 1992, A&AS, 96, 593
Leighly, K. M. 2000, NewA Rev., 44, 395
Mathur, S. 2000, MNRAS, 314, L17
Netzer, H. 2003, ApJ, 583, L5
Netzer, H., Brotherton, M. S., Wills, B. J., Han, M., Wills, D., Baldwin, J. A., Ferland, G. J., & Browne, I. W. A. 1995, ApJ, 448, 27
Netzer, H., Shemmer, O., Maiolino, R., Oliva, E., Croom, S., Corbett, E., & di-Fabrizio, L. 2004, ApJ, in press (Paper II)
Osmer, P. S., & Smith, M. G. 1977, ApJ, 213, 607
Peterson, B. M., & Wandel, A. 2000, ApJ, 540, L13
Peterson, B. M., et al. 2004, ApJ, 613, 682
Rodriguez-Pascual, P. M., Mas-Hesse, J. M., & Santos-Lleo, M. 1997, A&A, 327, 72
Romano, P., et al. 2004, ApJ, 602, 635
Shemmer, O., & Netzer, H. 2002, ApJ, 567, L19
Shields, G. A. 1976, ApJ, 204, 330
Stoughton, C., et al. 2002, AJ, 123, 485
Trager, S. C., Faber, S. M., Worthey, G., & González, J. J. 2000, AJ, 120, 165
Veron-Cetty, M. P., & Veron, P. 2003, VizieR On-line Data Catalog, 7235, 0
Vestergaard, M. 2002, ApJ, 571, 733
Wang, J.-M., & Netzer, H. 2003, A&A, 398, 927
Warner, C., Hamann, F., & Dietrich, M. 2004, ApJ, 608, 136
Wills, B. J., Laor, A., Brotherton, M. S., Wills, D., Wilkes, B. J., Ferland, G. J., & Shang, Z. 1999, ApJ, 515, L53
Wills, B. J., Netzer, H., Brotherton, M. S., Han, M., Wills, D., Baldwin, J. A., Ferland, G. J., & Browne, I. W. A. 1993, ApJ, 410, 534
Woo, J., & Urry, C. M. 2002, ApJ, 581, L5